

Ridged plains on Europa reveal a compressive past

E.J. Leonard^{a,b,*}, A. Yin^a, R.T. Pappalardo^b

^a Department of Earth, Planetary, and Space Sciences, University of California, Los Angeles 90095-1567, USA

^b Jet Propulsion Laboratory, California Institute of Technology, Pasadena, CA 91109, USA

ARTICLE INFO

Keywords:

Europa
Geological processes
Tectonics
Thermal histories
Experimental techniques

ABSTRACT

Europa's young surface implies relatively recent resurfacing. Ridged plains, which make up >50% of Europa's surface, have not yet been fully analyzed for a potential formation mechanism. Because ridged plains dominate Europa's surface, this terrain is key to understanding how Europa has resurfaced and how the resurfacing mechanisms may have evolved through time. In this work, we create a new high-resolution topographic model and a two-layer physical analog model to investigate the formation of ridged plains. We find that the ridged plains most closely resemble the compressional physical analog experiments which generate folds. Specifically, the analog experiments with a brittle layer <1/16th the thickness of the underlying ductile-layer best explain the morphological observations of the ridged plains on Europa. Based on the scaling relationships, we find that at the time of the ridged plains formation, the brittle part of the ice shell of Europa's ice shell was ~200 m thick and the total ice-shell thickness, including both the ductile and brittle parts, was >~3000 m. Compared to the predicted current ice shell thickness, this would imply that Europa's ice-shell has thickened through the visible surface history.

1. Introduction

Unlike most planetary surfaces in our Solar System, Europa is largely devoid of impact craters >10 km in diameter. Instead, its surface consists of several enigmatic features ranging from pervasive ridges and troughs to chaotic terrain resembling broken pieces of the ice shell (e.g., Greeley et al., 2000). Although the paucity of impact craters requires the surface age of Europa to be ~60 Ma (e.g., Schenk et al., 2003; Zahnle et al., 2003; Bierhaus & Chapman, 2009), the exact processes and mechanisms responsible for the resurfacing remain poorly understood. Current hypotheses addressing resurfacing on Europa range from cryovolcanism to plate tectonic processes (e.g., Crawford and Stevenson, 1988; Greenberg et al., 1998; Pappalardo et al., 1999; Greeley et al., 2000; Greenberg and Geissler, 2002; Figueredo and Greeley, 2004; Doggett et al., 2009; Kattenhorn and Prockter, 2014).

Analysis of stratigraphic relationships among major landform types suggests that the surface of Europa has been shaped by a three-staged development: (1) the initial formation of ridged plains, followed by (2) the development of band-like structures, and finally (3) the creation of chaos features (Greeley et al., 2000; Figueredo and Greeley, 2004; Leonard et al., 2018; Senske et al., 2019). The formation of the ridged plains (Fig. 1)—terrain consisting of overlapping subparallel to

crosscutting ridges and trough—is hypothesized to result from folding (Head et al., 1998; Patel et al., 1999; Leonard et al., 2018) or extensional faulting (Kattenhorn, 2002), but has not been widely investigated. The formation of band-like structures—discrete linear to curvilinear zones of deformation—has been attributed and extensional process similar to mid-ocean-ridge spreading on Earth (e.g., Prockter et al., 2002; Prockter and Patterson, 2009). The spreading hypothesis is consistent with predicted band morphology and reconstructions of pre-band-formation structures that require significant ice-shell separation (Schenk and McKinnon, 1989; Sullivan et al., 1998; Prockter et al., 2002; Prockter and Patterson, 2009). The formation of chaos—terrain consisting of blocks of preexisting terrain and hummocky matrix material—has been intensely debated over time, with end-member hypotheses including melt-through, sill formation and collapse, and diapirism induced by thermal and/or chemical buoyancy (Pappalardo et al., 1998; Greenberg et al., 1999; O'Brien et al., 2002; Collins and Nimmo, 2009; Schmidt et al., 2011; Michaut and Manga, 2014). Individual ridges form throughout the stratigraphic sequence (e.g., Figueredo and Greeley, 2004; Senske et al., 2018) and, from regional-scale mapping, are noted to gradually increase in size and become more prominent with time (Figueredo and Greeley, 2004).

The aforementioned hypothesis for three-stage development of the

* Corresponding author at: Jet Propulsion Laboratory, California Institute of Technology, Pasadena, CA 91109, USA.

E-mail address: Erin.J.Leonard@jpl.nasa.gov (E.J. Leonard).

geology on Europa requires ice-shell deformation to have transitioned from a distributed (widespread strain and deformation) to a discrete mode (focused strain and deformation), possibly caused by progressive ice-shell thickening in combination with tidal stresses since the onset of a global resurfacing event (Pappalardo et al., 1999; Figueredo and Greeley, 2004; Leonard et al., 2018). If the ice shell thickening stressed dominated deformation, we would expect the formation mechanisms for surface features to transition from compressional to extensional as the ice-shell thickens (Nimmo, 2004). Alternatively, the ice-shell could be in steady state with deformation induced by tidal stresses and/or nonsynchronous stresses (e.g., Greenberg et al., 1998; Greenberg et al., 2002). In the latter scenario, the evolution of ice-shell structures through time is not recognized and therefore it is required that all surface structure types can be formed at essentially the same time. Differentiating between these competing hypotheses for Europa's surface evolution requires better understanding of how the ridged plains formed, as they set the initial conditions for the subsequent or contemporary resurfacing processes: ice-shell thickening would require the ridged plains to be contractional in origin when thermal contraction effects dominate over volume expansion (Nimmo, 2004), whereas tidal forcing and nonsynchronous stresses have stress fields that rotate with time and therefore would predict the ridged plains to have been generated by some combination of extensional, compressional, and strike-slip deformation (Hoppa et al., 1999a, cf. Sarid et al., 2002).

Some of the best imaged ridged plains features are those mapped by Leonard et al. (2018) using the highest resolution images available for this type of terrain. In the present work, we use the term "ridged plains" to refer to four of the five morphologies that have been recognized in high-resolution images (<50 m/pixel; e.g. Fig. 1) of Europa (Patel et al.,

1999b; Leonard et al., 2018) all of which are variations of a subparallel, systematic ridge-and-trough terrain (as opposed to the fifth morphology, "mélange" which is a subtype of ridged plains that consists of many overlapping ridges and troughs). Although Leonard et al. (2018) favored a contractional origin for the ridged plains analyzed in their study (Table 1), similar Europa structures were alternatively interpreted as resulting from related extensional block faulting (Kattenhorn, 2002), akin to the detachment model for the grooved terrain development on Ganymede (Pappalardo and Greeley, 1995; Patel et al., 1999; Prockter et al., 1998, 2000; Figueredo and Greeley, 2004). One possible way of differentiating between the two competing models of Europa surface evolution (i.e., compression versus extension) is to explore the mechanical controls for the morphological development of the ridged plains. Specifically, rigorously scaled analog experiments under contrasting boundary conditions create ridged surface morphologies that

Table 1

Comparison of subparallel ridge-and-trough (ridged plains) formation mechanisms against observations in the high-resolution mosaic [modified from Leonard et al., 2018].

	Tilt-blocks	Folds
Symmetric ridges	N	Y
Shallow slopes	Y	Y
Linear or curvilinear	N	Y
Can bifurcate	N	Y
Systematic	Y	Y

Note: "Y" indicates where theory satisfies the observation, and "N" indicates where it is unclear or not satisfied. Modified from Leonard et al. (2018).

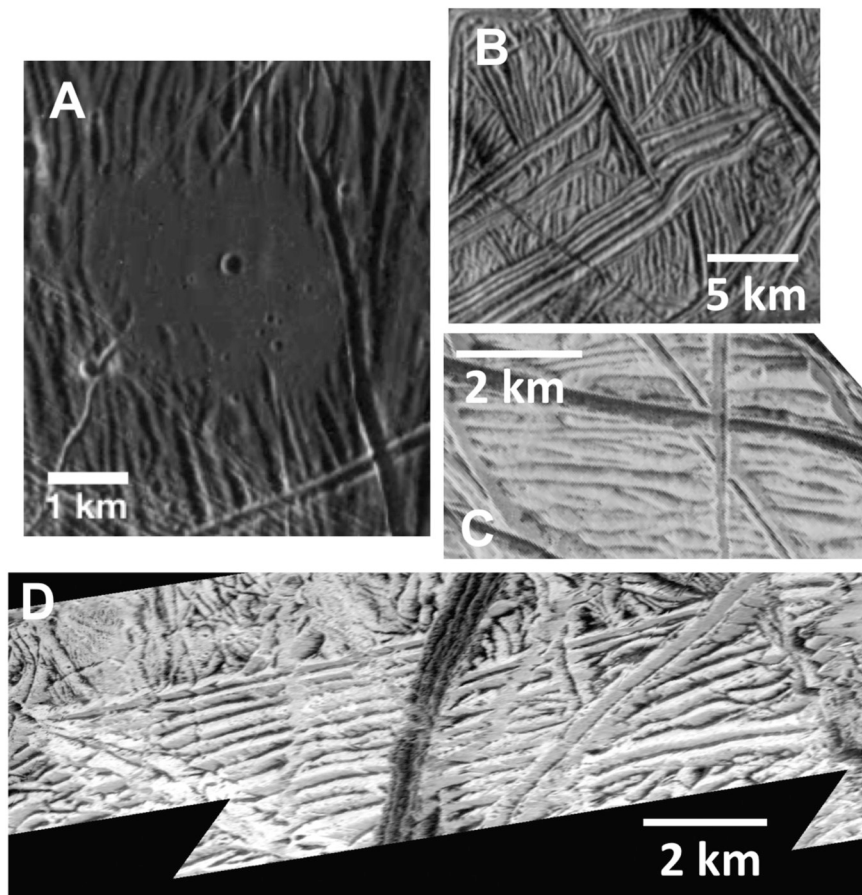


Fig. 1. A variety of examples of ridged plains on Europa. Note the linear to curvilinear systematic ridge traces in all examples: (A) frame 5452 at 26 m/pixel from the Galileo E4 flyby of Europa, (B) frame 8700 at 66 m/pixel from the Galileo E19 flyby of Europa, (C) frame 2821 at 29 m/pixel from the Galileo E12 flyby of Europa, and (D) frames 2400–2405 at 16 m/pixel from the Galileo E12 flyby.

can be compared against ridged plains morphologies observed in the high-resolution images (e.g., Fig. 1) and the resulting topographic data.

In this study, we first developed a two-layer physical analog model using an experimental setup constructed at the University of California, Los Angeles. We then created stereo-topography data of E12 Galileo SSI images of ridged plains, and compare our experimental results together with the highest resolution satellite images. A key result of the work is that the compression-induced morphology best explains the observed map pattern and inferred cross-sectional shapes of the ridged plains features. The ridged plains are among the oldest features on Europa and we hypothesize that these features are formed through contractional deformation. Because, stratigraphically, ridged plains formation is followed by the formation of younger extensionally induced band structures (Leonard et al., 2018), we suggest that this sequence of events can simply be explained by progressive ice-shell thickening due to secular cooling of the ice-shell and ocean system.

2. Data and methods

2.1. Topographic data and morphologic observations

One of the few regions the Galileo mission imaged at a sufficient resolution (<50 m/pixel) to analyze the ridged plains, is the E12 MOTTLE region, occurring on the Trailing Anti-Jovian hemisphere and near the equator of Europa. Because of the lack of imaging at resolutions <50 m/pixel, we must assume that ridged plains around Europa have a similar morphology. However, the E12 MOTTLE region (Fig. 1D) is thought to capture typical terrain types on Europa due to its location on

the border between large regions of chaos and ridged plains (see Leonard et al., 2018 for further description) and similarity to the few other high-resolution regions (see Fig. 1). While we assume this region is representative of the ridged plains unit on a global scale, it is important to note that this could not be the case, affecting the resulting conclusions, but further data is needed to verify this assumption.

We produce stereo-topography data from the image frame overlaps of the Galileo SSI E12 MOTTLE images (specifically, image frames 2400 and 2404; Fig. 2) using the Ames Stereopipeline software (Broxton and Edwards, 2008; Moratto et al., 2010). The initial resolution of these images is 16 m/pixel. The small angle change between the images ($\sim 0.2^\circ$) is non-ideal for constructing the digital topographic models. To minimize the error as much as possible, we average three topographic profiles spaced at ~ 100 m (Fig. 2C), which shows the amplitudes of individual ridges to be 50–80 m (Fig. 2D). The horizontal resolution of the DEM (Fig. 2D), ~ 125 m/pixel, which could contain sub-resolution structure that is not resolved due to the noise resulting from the small angle change in the images.

We combine the information from the resulting Digital Elevation Model (DEM) and the images themselves to determine the height and spacing of the ridges. From these measurements, we calculate the linear strain, ϵ [%] = $100 * \frac{L - L_0}{L_0}$ where L is the final length (half-wavelength of the ridge) and L_0 is the original length or ridge slope length. This calculation assumes that the undulating surface started as a perfect plane later deformed by extension as tilted blocks or compression as folds.

The ridged plains subunits in the E12 MOTTLE region display the

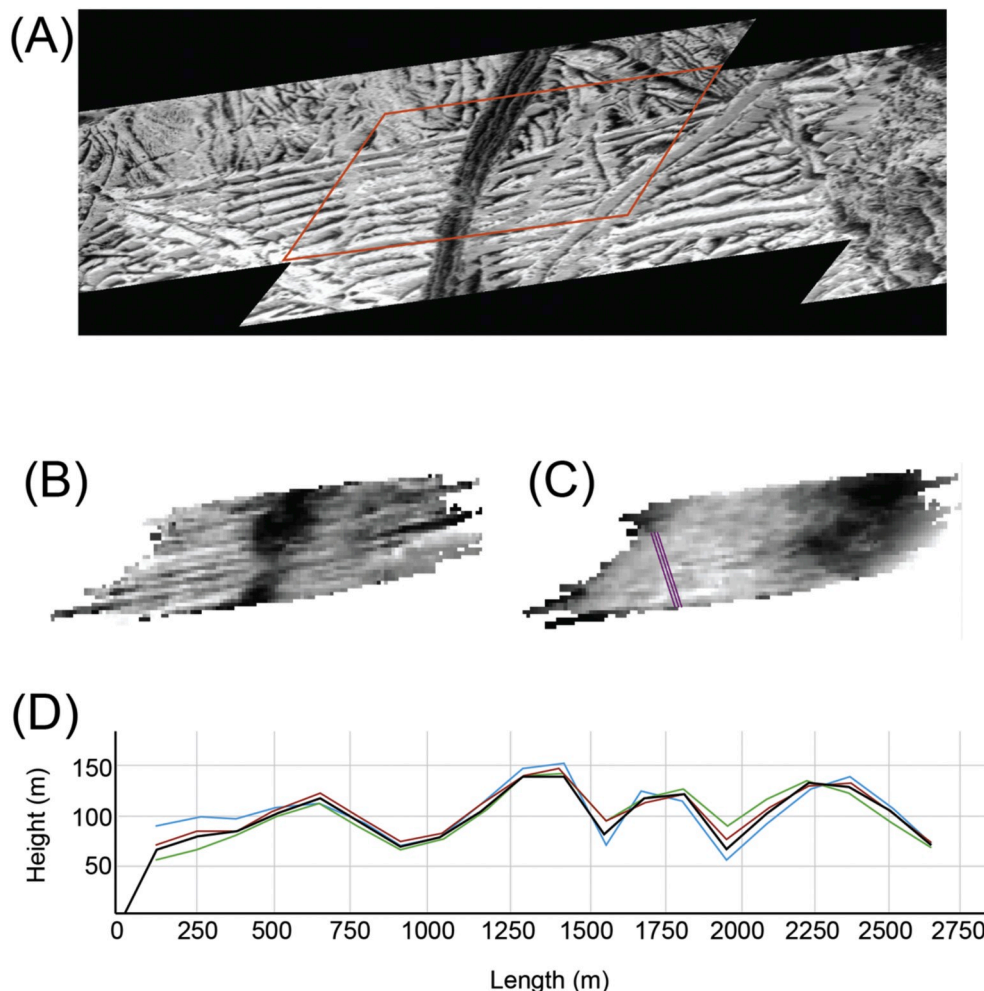


Fig. 2. (A) Location of stereo-topography outlined in a red box, frames 2400–2405 from the Galileo E12 flyby. (B) Image overlain with topographic product. (C) Digital elevation model with lines indicating the approximate location of topographic profiles in (D), where white shades are topographically high and darker shades are topographically low. (D) The topographic profiles from (C), where the black line is the average of the three topographic profiles. (For interpretation of the references to color in this figure legend, the reader is referred to the web version of this article.)

following characteristics (Leonard et al., 2018) (Table 1): (1) the presence of symmetric shallow slopes, (2) curvilinear to sinuous traces of individual ridges along their length, (3) ridge bifurcation along the general ridge trend, and (4) a sub-parallel trend for an individual ridge-and-trough set. In the limited high-resolution area mapped by Leonard et al. (2018), the individual ridges are relatively consistent at 300 ± 100 m wide and a length-to-width ratio of >10 . The total width or length of a ridge-and-trough set cannot be determined with the current data due to the limited extent of the high-resolution images (e.g., Fig. 1D). Some of the troughs separating each ridge contain a low albedo material, potentially emplaced by ice sublimation or downslope mass wasting processes (Spencer, 1987).

2.2. Experimental setup and procedures

Although analog models have been widely applied for tectonic studies on Earth (e.g., Davy and Cobbold, 1988; Maillot and Koyi, 2006; Cruz et al., 2008), they were rarely used for the studies of ice-shell deformation (cf., Manga and Sinton, 2004; Sims et al., 2014). In this work, we model the ice-shell of Europa consisting of lower ductile warm ice and upper brittle cold ice. We use a ductile putty layer to simulate the lower-crustal ductile deformation and a sand layer to simulate the upper-crustal brittle deformation. The experimental ductile material is a therapeutic putty with a viscosity of $\sim 10^4$ Pa s, that is Newtonian at small strain rates ($< \sim 10^{-4}$). For the brittle layer, we use a fine-grained ($< 200 \mu\text{m}$) dry sand with a cohesive strength of ~ 60 Pa and a frictional angle of $22\text{--}27^\circ$ (Zuza et al., 2017). Using the ratio between the cohesive strengths of ice on Europa (Beeman et al., 1988) and of the dry sand (Zuza et al., 2017) used in the experiments, we obtain a length scaling factor of $1:10^{-5}$ based on the scaling law of Hubbert (1937) (and also see its application by Cruz et al., 2008 for analyzing terrestrial structural deformation):

$$\frac{h_{ice}}{h_{mod}} = \frac{C_{ice}}{C_{mod}} \cdot \frac{g_{mod}}{g_{ice}} \cdot \frac{\rho_{mod}}{\rho_{ice}} \quad (1)$$

where the subscript *ice* refers to Europa and the subscript *mod* refers to the analog model values, h is the thickness of the brittle layer, C is the cohesion of the brittle layer, g is the gravity, and ρ is the density of the brittle layer material. This scaling law implies that a 1-cm thick sand layer in our model on Earth represents an about 2-km thick ice shell on Europa. The time scaling factor was obtained by using the ratio between the putty viscosity and average viscosity of warm ice assumed to be 10^{14} Pa s (e.g., Poirier, 1982; Showman and Han, 2004; Mitri and Showman, 2005) using the relationship proposed by Davy and Cobbold (1988):

$$\frac{t_{ice}}{t_{mod}} = \frac{\mu_{ice}}{\mu_{mod}} \cdot \frac{h_{mod}}{h_{ice}} \quad (2)$$

where t is the duration of deformation, and μ is the viscosity of the ductile layer. This leads to a scaling factor of $1:10^{-9}$, where a 24-h experiment corresponds to a deformation episode of $\sim 10^6$ years on Europa. The boundary between the brittle and ductile layer in our experiment is discreet, as opposed to the likely more gradual transition on Europa, which means we are modeling an end-member behavior of this system where the transition occurs abruptly, perhaps due to a well-mixed ductile layer (e.g., through vigorous convection). Additionally, there is no discreet elastic layer in our experiment, much like in nature where there is no physical or geologic boundary that defines an elastic layer (Burov and Diament, 1995). An elastic layer is partially defined based on the strain rate of deformation. However, we are modeling low strain rate deformation, where we expect the ice shell on Europa (and also our experiment) to deform viscously.

To set up an experimental run, we first place the putty into an analog experimental box made of aluminum plates with movable walls used for imposing bounding conditions (Fig. 3). The boundary at the bottom of the box is not lubricated in these experiments and we will show later that

the interface of importance to the results is the location of the sand-putty interface (see Section 3.2.2). We let the putty relax to a flat surface over the course of 3–7 days before sifting the sand onto the putty until the desired sand thickness (0.25–1 cm) is reached. Finally, we scatter coffee grounds over the surface of the sand that act as tracking particles of surface deformation during the experiment (after Riller et al., 2012). In order to run an experiment, we employ a step motor to move a wall to either compress or extend the layered experimental materials at a constant rate, which is calculated from the ratio of the length and time scaling factors as shown in Table 2.

3. Results

3.1. Linear strain

In addition to the morphological characteristics of ridged plains identified by Leonard et al., (2018), our newly generated topographic data (Fig. 2D) show that individual ridges have amplitudes varying from 50 m to 80 m. Observed ridge flanks are symmetrical, with an average angle of $10\text{--}20^\circ$ (Fig. 2D). The ridges analyzed in the DEM have a wavelength of 400–600 m (Fig. 2D). Erosion, via sputtering for example, of the ridges is thought to be negligible (e.g., Pappalardo et al., 1999) so this topography represents the formational state of the ridges. Using the methods described in Section 2.1, we find a compressional strain associated with the ridged plains formation of 3–7%. This is a first-order calculation because it assumes an original flat surface folded into a ridge that is triangular in cross-section, pure-shear shortening (perpendicular to the ridge), and it does not consider the contribution of other mechanisms (e.g., thickening, cleavage formation, etc.).

3.2. Experimental results

The brittle sand layer thicknesses used in the experimental runs are 0.25 cm, 0.5 cm, and 1.0 cm whereas the ductile-layer thicknesses are 2 cm, 6 cm, and 8 cm, for a total of nine potential variations in model setup before imposing either extension or compression. The moving wall simulating the horizontal boundary induces an averaged strain rate of 10^{-6} s^{-1} , which scales to a strain rate of $\sim 10^{-15} \text{ s}^{-1}$ on Europa (Eq. 2). Note that there is nothing holding the putty to the experimental box wall, but that the 10^{-6} s^{-1} strain rate was chosen because it closely matches the viscous flow of the putty. We run each experiment for 24 h, resulting in $\sim 30\%$ total strain (uninterpreted in Fig. 4A and interpreted in Fig. 4B). Prior to deformation, the surface of the analog model is generally smooth with coffee grounds scattered on top to act as strain markers (Fig. 4A and B, i and v). Ridges, in both compression and extension, begin to emerge across the deformation region within the first 8 h of the experiment, or around 10% strain (Fig. 4A and B, ii, and vi). As deformation proceeds, the ridged become increasingly well-defined and closely spaced (Fig. 4A and B, iii, iv, vii, and viii).

After the duration of the compressional experiment, we observe that the ridge traces generated are linear to curvilinear, spaced regularly, bifurcated, and bounded by narrow troughs. The resulting morphologies of our compressional ridges agree well with results of similar experiments scaled for Earth (e.g., Dubey and Cobbold, 1977). Interestingly, the region proximal to the moving wall in the compressional experiments does not show any surface deformation. In the extensional experiments, the ridges (horsts) are wide with flat tops (Fig. 4) and the troughs (graben) between each ridge are wide and generally evenly spaced. After the completion of the experiment, the features relax on a long timescale (>1 week), but do not completely relax away (on an observable timescale).

3.2.1. Varying brittle layer thickness

The first variation we test in the analog experiments is different brittle layer thicknesses, while holding the ductile layer thickness constant at 2 cm. In the experiments with a compressional boundary

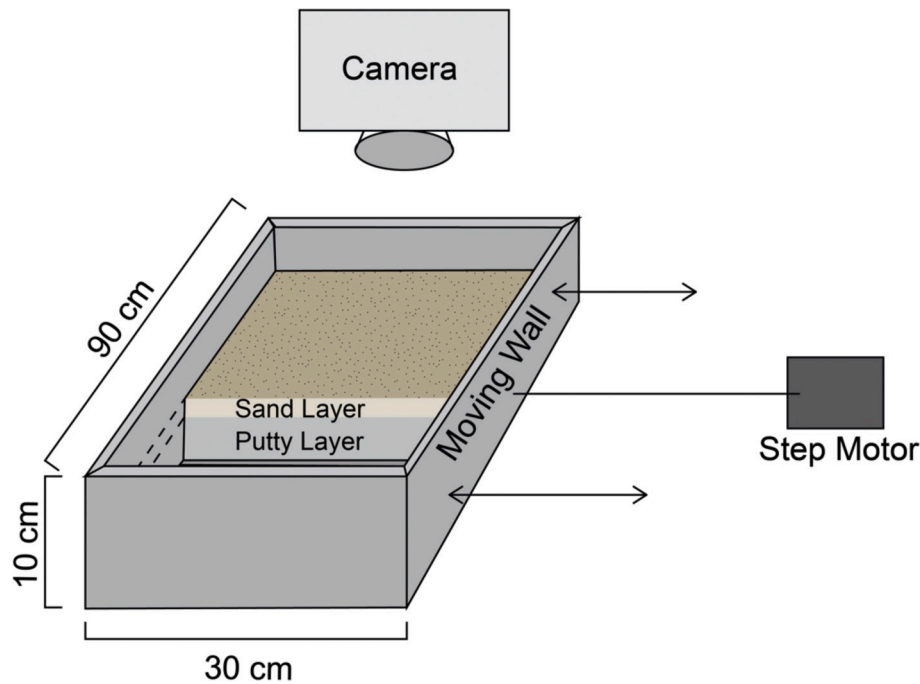


Fig. 3. Schematic of the physical analog model set-up. The moving wall on the right is controlled by a step-motor that we control using the LinControl computer software. The camera above the experimental set-up takes pictures of each experiment at 2-min intervals.

Table 2
Material values for the analog experiments, and for Europa.

Material property**	Experiment value	Europa value*
Cohesion, C	60 Pa	10^6 Pa
Density, ρ	1700 kg/m^3	920 kg/m^3
Gravitational acceleration, g	9.8 m/s^2	1.31 m/s^2
Height scale, h	1 cm	2 km
$\frac{h_{ice}}{h_{mod}} = \frac{C_{ice} \rho_{mod} g_{mod}}{C_{mod} \rho_{ice} g_{ice}}$		
Viscosity, μ (ductile)	10^4 Pa s	$10^{17}\text{--}10^{18} \text{ Pa s}$
Time scale, t	24 h	10^6 years
$\frac{t_{ice}}{t_{mod}} = \frac{\mu_{ice} C_{mod}}{\mu_{mod} C_{ice}}$		

* Values found in: Beeman et al. (1988); Pappalardo et al. (1999); Prockter and Pappalardo (2000); Zuza et al. (2017).

** Equations from Hubbert (1937) and Cruz et al. (2008).

condition, the wavelength of the resulting folds and the spacing of the resulting thrusts increase with the brittle-layer thickness (Figs. 5 and 6). The ridges that formed in such experiments display a square to rounded cross-sectional shape (Fig. 7). However, the emergence of the rounded geometry depends critically on the thickness of the ductile layer when the thickness of the brittle layer is fixed (see Section 3.2 below).

In the extensional experiments, the spacing of the resulting normal faults increases with brittle-layer thickness (Figs. 5 and 6). This result is consistent with the predictions of the infinitesimal-strain instability models (e.g., Fletcher and Hallet, 1983; Yin, 2000). However, we could not run the extensional experiments with a brittle layer thickness of 0.25 cm because the resulting structures are below a visible resolution ($< 2 \text{ mm}$) and likely have strong influences from the grain size of the sand. None of the extensional experiments produce tilt blocks, possibly due to insufficient basal shear to create the detachment fault within the sand layer (e.g., Wainwright and Brun, 1999).

3.2.2. Varying ductile layer thickness

We systematically change the ductile-layer thickness to determine its effect on surface structures. This set of experiments was motivated by the work of Stewart (1996) who proposed that the thickness of a ductile

substrate determines whether folds or thrusts occur in the overlying brittle layer. Using a 2 cm thick layer of the putty places the experiments in the regime of mixed folds and thrusts according to the empirical relationship proposed by Stewart (1996) model (Fig. 8). Thus, this work not only assesses how ductile layers affect the surface development of ice-shell structures, but also will independently test the postulation by Stewart (1996).

The extensional experiments show that the surface morphology of the resulting structures does not change with the ductile-layer thickness. This indicates that even increasing the potential shear between the brittle layer and the ductile layer does not produce enough shear to form the listric fault or decollement needed to produce tilt-block style extensional deformation. Therefore, we conclude that tilt-blocks cannot be formed under the conditions imposed by this experiment and will not form on Europa unless other deformational mechanisms are invoked (e.g., uplift or topographic induced sliding).

The compressional experiments, however, transition from thrust-dominated structures to fold-dominated structures as the ductile layer thickens (Figs. 9 and 10). This is accompanied by a change in the cross-section shape from asymmetric, to box-fold like, to a cylindrical syncline as the ductile layer thickens (Fig. 9). The spacing of the ridges decreases initially with increasing ductile-layer thickness (2 cm to 6 cm; Fig. 9A–C) and plateaus during the continued thickening (6 cm to 8 cm; Fig. 9D) (cf. Martinod and Davy, 1994).

4. Discussion

The thickness of the ductile layer has an effect on the resulting structures generated within the analog model (Fig. 9). From our set of experiments, we generate a regime diagram (Fig. 10) indicating when folds (F) versus when thrusts (T) dominate the surface structures, as inferred from cross-sections produced from each experiment. Increasing the ratio of the ductile-layer to brittle-layer thickness changes the structural mechanism that results in the ridges, and it changes the cross-sectional shape (Fig. 9). As folding begins to dominate, the ridges become increasingly rounded in cross-section, which matches the observed morphology of ridged plains on Europa (Fig. 11; Table 3). The ridges are not always linear or regular, but linearity and regularity

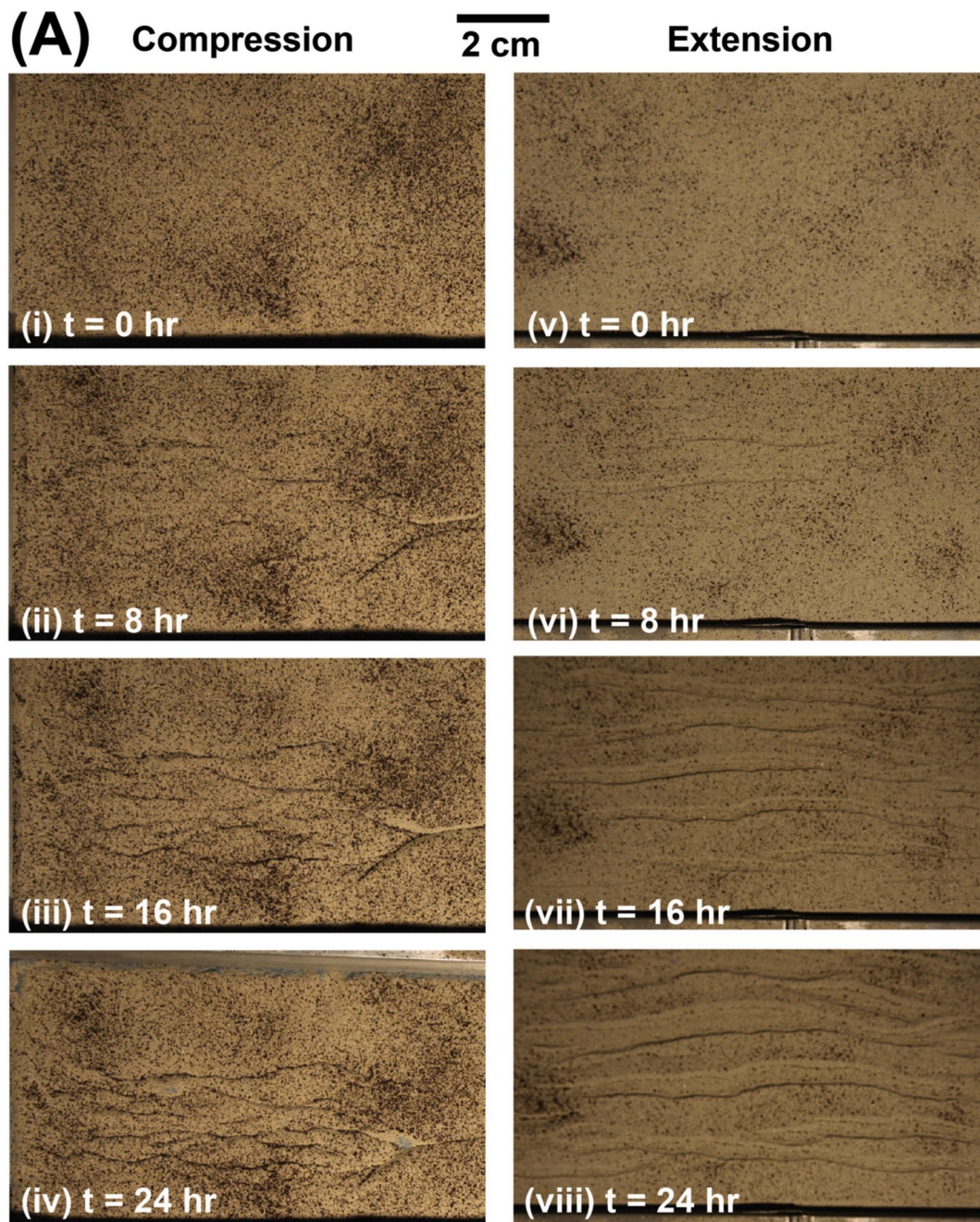


Fig. 4. Images (A) and interpretations (B) of a compressional experiment (0.5 cm brittle layer, 2 cm ductile layer) and an extensional experiment (1.0 cm brittle layer, 2 cm ductile layer), each over the course of 24-h deformation period. The moving wall, which will compress or extend the analog model, is toward the top of each image. The top row of images (i and v) is the initial analog model set-up, prior to any deformation. The second (ii and vi), third (iii and vii), and fourth (iv and viii) rows are after 8, 16, and 24 h of deformation respectively. The final row is also after 24 h of deformation (at the end of the experiment), but without the superimposed structural interpretation. Note how between 16 and 24 h, the only significant difference is in the spacing of the resulting structures and the ridges in the compression experiments increase in linearity.

appears to increase as sand thickness decreases (compare Fig. 4 to Fig. 11). Thus, while we do not observe the degree of regularity in the experiments that we observe in the ridges on Europa (Fig. 11), we predict that regularity and linearity of the ridges would continue to increase as the brittle layer thickness is decreased.

Because the observed morphology of ridges in the thick ductile layer compressional experiments more closely match the observations of ridged plains on Europa (Table 3; Fig. 11) when compared to the extension-generated ridges, we find that folding is likely the formation mechanism for the ridged plains. In particular, while the ridges

generated in the extensional experiments can appear rounded in cross-section as the brittle layer thickness decreases (Fig. 11C), we interpret this as an effect of the grain size of the sand with respect to the scale of the ridges (i.e., only a few sand grains make up the shape of the extensional ridge, effecting the shape). Additionally, the extension experiments do not produce ridges with shallow slopes or narrow troughs, like the observed ridges in the ridged plains on Europa (Fig. 11C). Thus, we interpret the ridged plains to be formed through folding. In order for folding to dominate, we find that the brittle layer must be thinner than one sixteenth of the combined brittle-ductile layer thickness (Fig. 10).

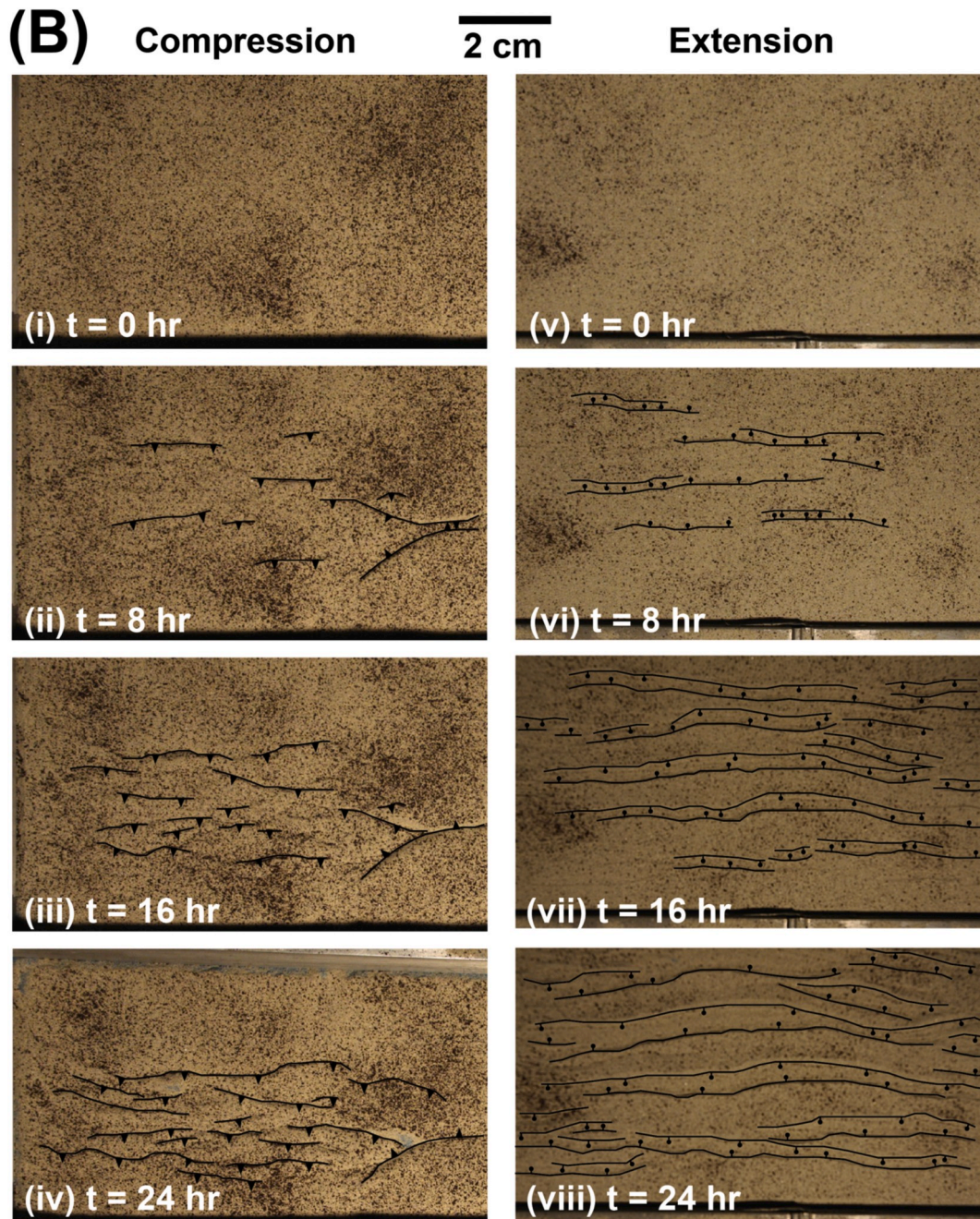


Fig. 4. (continued).

When scaled to Europa (Eq. (1)), the result requires the corresponding brittle ice layer to be ~ 200 m thick and the total thickness of the ice shell to be greater than ~ 3000 m during the development of the ridged plains.

We can also calculate the linear strain produced in the physical analog experiments under compression with a thick ductile layer, using the same method we used for the ridged plains in Section 3.1. Assuming a triangular shape for each ridge in the experiment in Fig. 9, results in a linear strain of 4–9%, similar to that inferred from the ridged plains (see Section 3.1). Note that the total shortening in the experiments is made up of two components: (1) uniform shortening and accompanied layer thickening (i.e., basic strain as described by Smith, 1975), and (2) shortening accommodated in folds generated from instabilities between the brittle and ductile layer (Smith, 1975). Only the latter component of the strain can be determined using the topographic profiles, here and in Section 3.1, assuming the ground surface before deformation was a flat

plane. We do not recover the input strain of $\sim 30\%$ in the experiments because there is also deformation going in to thickening the ductile layer, not just creating the observed ridges. Therefore, it is likely that the folds generating the ridged plains on Europa require more than the observed strain from topography, as there was likely ductile layer thickening as well.

Folding as a possible mechanism of ridged plains formation has important implications for the evolution of Europa, as this is the oldest preserved unit on the icy moon, and its history provides key information about the initial conditions of the latest global resurfacing event. For example, a fold origin requires compression to dominate ice-shell tectonics at the onset of the presumed resurfacing event. This agrees with the general three-stage evolution of Europa's surface (e.g., Figueredo and Greeley, 2004; Leonard et al., 2018), as opposed to the continuous formations of all feature types (e.g., Greenberg & Geissler, 2002). Thus,

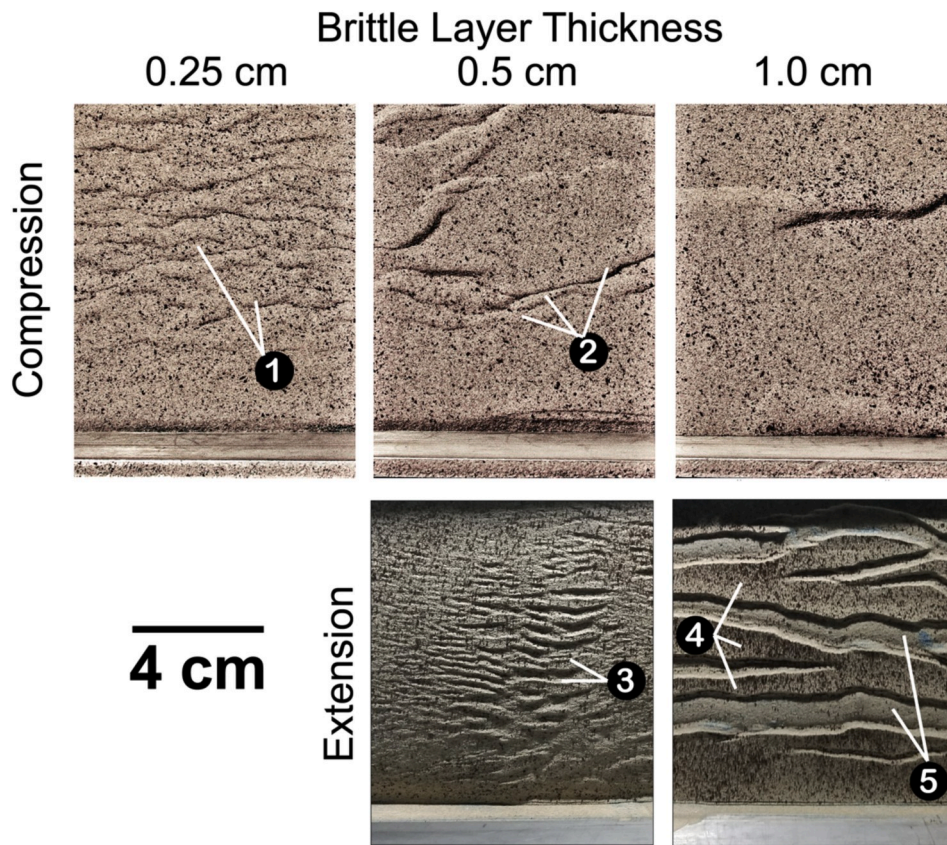


Fig. 5. Experiment results with constant ductile layer thickness at 2 cm and varying brittle layer thickness of 0.25 cm, 0.5 cm, and 1.0 cm. The numbers indicate key features of the experimental results: (1) the rounded geometry of the compressional ridges, (2) the curvilinear trace of the features, (3) the steep slopes and flat-top geometry of the extensional ridges, (4) the horsts/ridges, and (5) the graben/troughs.

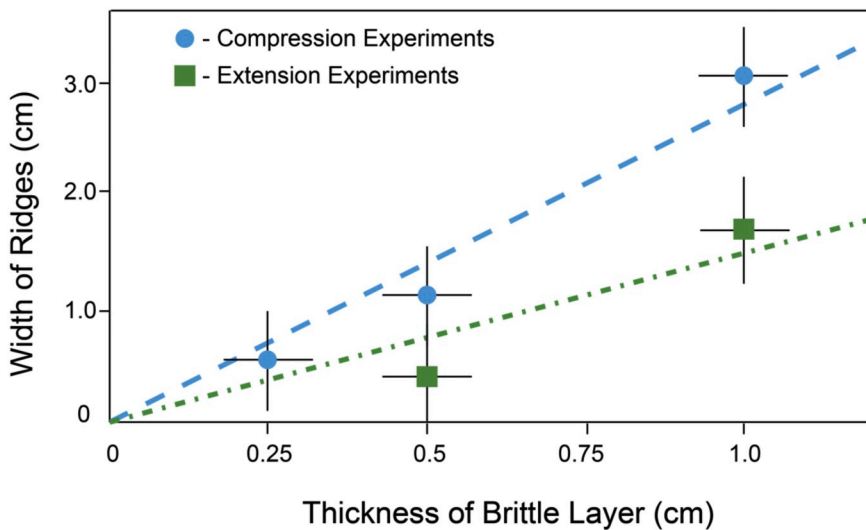


Fig. 6. Graph of the experiment results showing how the width of ridges varies with the thickness of the brittle layer. The blue circles are the data points from the compression experiments, and the green squares are the data points from the extension experiments. There error bars are set at ± 0.5 cm to capture the varying widths of the ridges across a single experiment. (For interpretation of the references to color in this figure legend, the reader is referred to the web version of this article.)

the hypothesis that the more recent ice deformation (e.g., band formation) is dominated by extension (e.g., Prockter et al., 2002; Prockter and Patterson, 2009) indicates that there must have been a transition time when the ice-shell deformation changed from compression to extension. We suggest that this change in the mode of deformation resulted from progressive cooling and thickening of the ice shell originating from a thin frozen layer over a global ocean. Specifically, the early but brief volume contraction in the shallow part of the ice shell (Nimmo, 2004) led to uniform contraction and folding; later and protracted volume

expansion created the younger extensional structures. However, we note that the strain to form the ridged plains, as estimated from our experiments, is an order of magnitude higher than what is predicted by ice shell thickening (Nimmo, 2004). It is possible that the surface of the satellite had extensional and compressional tectonics simultaneously during the transition stage, which allowed the high shortening strain expressed by the formation of the ridged plains to have been accommodated by local extension elsewhere. Alternatively, other global stress mechanisms—such as tidal stress, nonsynchronous stress, or obliquity

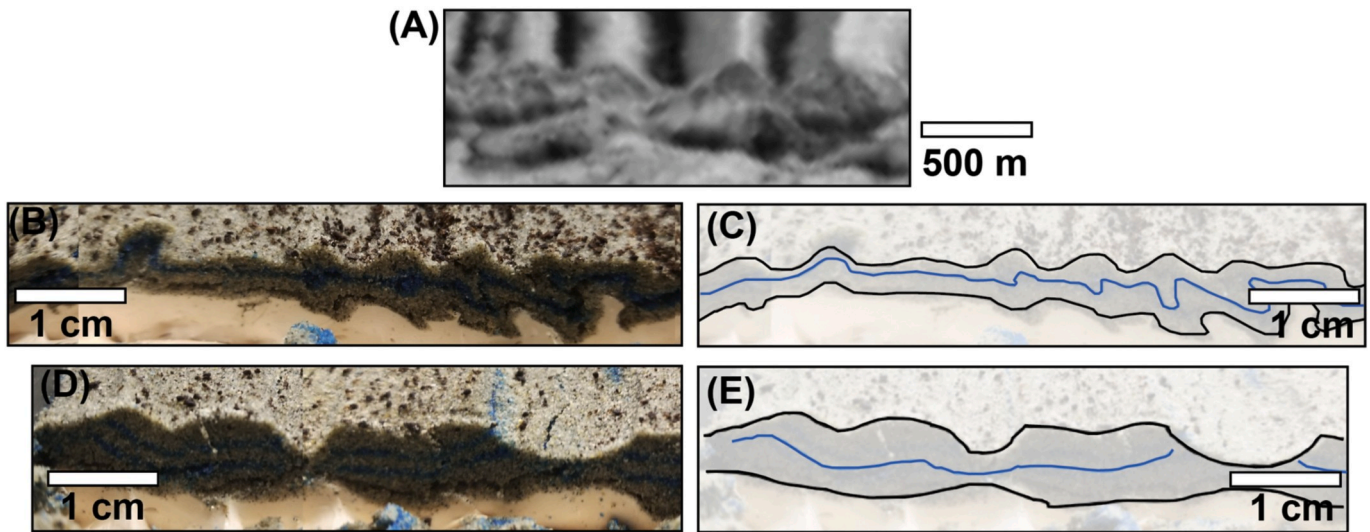


Fig. 7. Experiment results compared to ridged plains terrain in cross-section view. The top panel (A) is part of Frame 1989 from the E12 MOTTLE Galileo SSI data, illustrating the subparallel ridge-and-trough morphology of the ridged plains cut by a scarp, so that we see the ridges in cross-section. The middle panels (B) and (C) show the cross-section of a compression experiment with 0.5 cm brittle layer and 8 cm ductile layer where (B) is the uninterpreted version of (C). The bottom panels (D) and (E) show the cross-section of an extensional experiment with 0.5 cm brittle layer and 2 cm ductile layer where (D) is the uninterpreted version of (E).

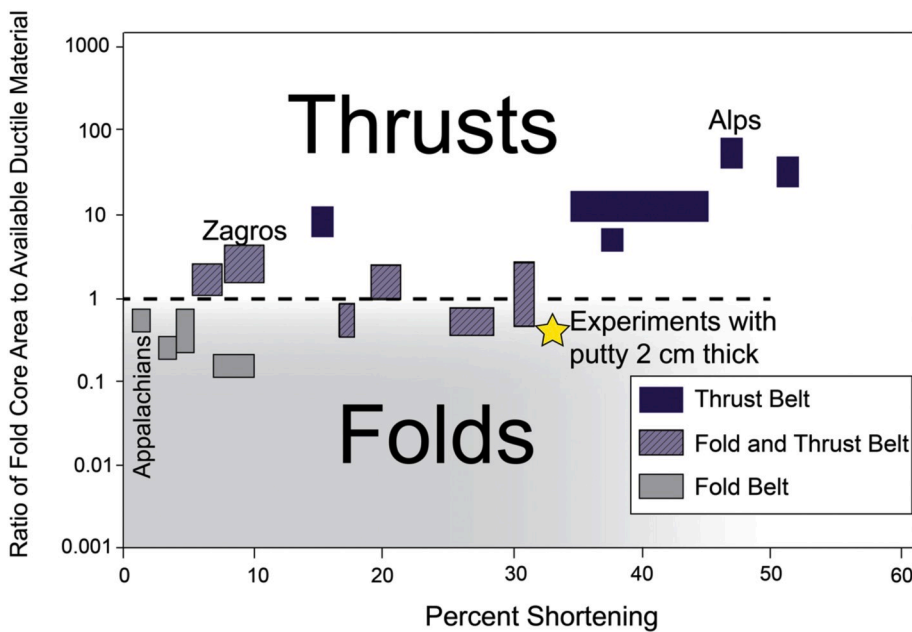


Fig. 8. Regime diagram for the formation conditions for folds versus thrust faults [Modified from Stewart (1996)]. The yellow star shows where our experiments sit when the ductile layer is 2 cm thick. When we increase the ductile layer thickness (to 6 cm and 8 cm), the star would move down further into the folds regime, resulting in more folds and fewer thrusts in our experiments. (For interpretation of the references to color in this figure legend, the reader is referred to the web version of this article.)

stress—may contribute to the deformation of the ridged plains and further modeling of how these stresses would interact is needed. Additional detailed mapping of high-resolution Galileo images, and a greater understanding of ice deformation at relevant temperatures and scales, may also aid in determining how the contractional strain required for ridged plains formation is induced.

This hypothesis may be tested by the new data to be returned by the planned Europa Clipper mission (Phillips and Pappalardo, 2014). For instance, the presence of a non-ice layer in the near-surface of the ice-shell (possibly detectable by REASON, the radar instrument) could indicate that the ice shell was thinner before re-freezing rapidly to entrain increased concentrations of non-ice and cause compression in the near surface (Leonard and Howell, 2019). Additionally, high-resolution (<50 m/pixel) images provided by EIS, the camera instrument, would allow for further characterization of the ridged plains at a

global rather than local scale, revealing whether the region analyzed in this manuscript is actually representative of ridged plains material globally. Additionally, high-resolution imagery over a broader region and associated topographic data would allow for further constraints on strain estimates for the formation of ridged plains.

5. Conclusions

Comparing the observations of ridged plains on Europa to the surface structures generated by our analog experiments, we find that the resulting ridge-trough systems in the compressional experiments match best the observed cross-sectional shape and map-view patterns of Europa's structures. This result leads us to suggest that the ridged plains resulted from global cooling associated with an initial volumetric expansion of the ice crust at the onset of the latest resurfacing event,

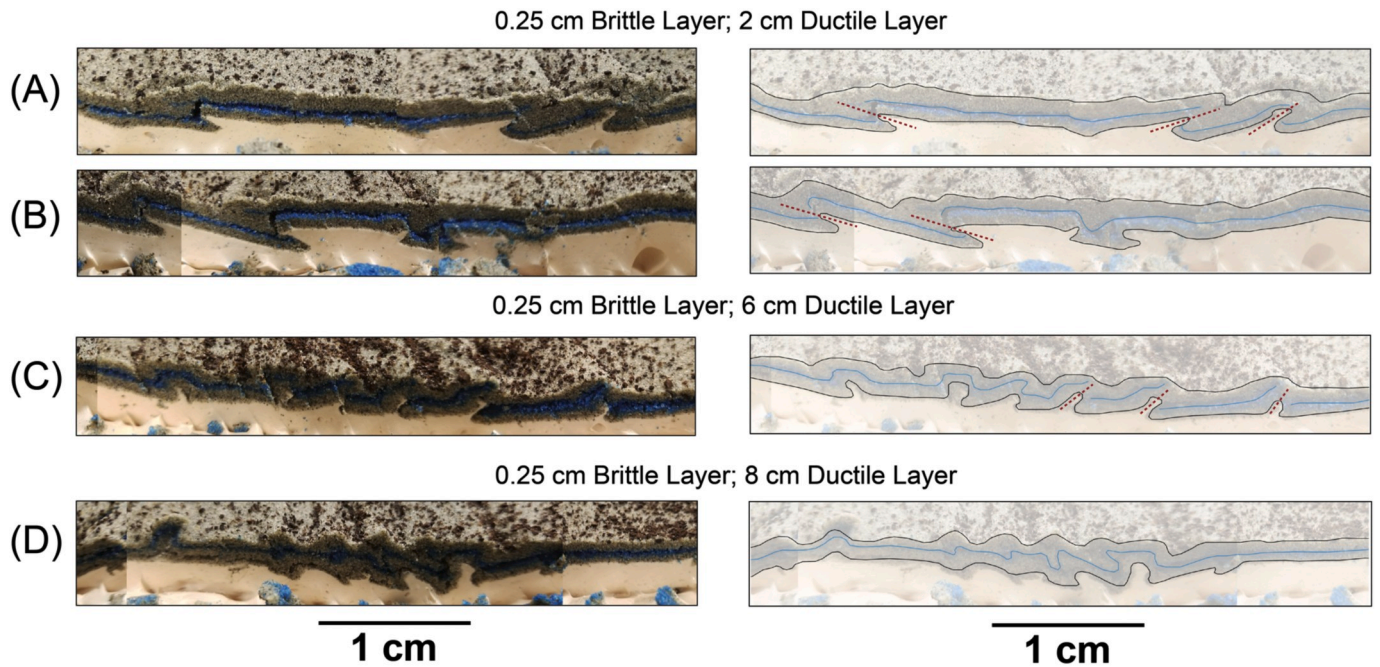


Fig. 9. Cross-sections of different compressional experiments with constant brittle layer thickness (0.5 cm) and varying ductile layer thickness (2 cm – (A) and (B), 6 cm – (C), and 8 cm – (D)). The images on the left are the uninterpreted versions of the images on the right. Note how the dominate ridge formation mechanism transitions from thrusting to folding as the ductile layer thickness increases. The red dashed lines in the right column of images indicate the approximate location of a thrust fault. (For interpretation of the references to color in this figure legend, the reader is referred to the web version of this article.)

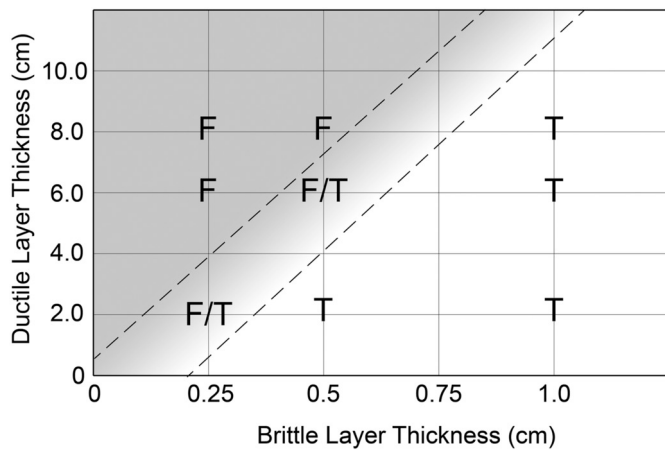


Fig. 10. A regime diagram for our experiments, showing where the brittle layer thickness to ductile layer thickness ratio will result in a transition from a thrust-dominated (T) to fold-dominated (F) environment.

resulting in an average surface age of ~60 Ma. This was followed by ice-shell extension expressed by the formation of band structures. A major requirement for this model is that the last global resurfacing process started from the entire satellite covered by a thin ice shell over a global ocean, and its progressive cooling (and possibly with the perturbation of tidal stresses) has led to the three-state evolution of the surface structures on Europa. Our results imply that the initial brittle layer of the ice shell during the development of the ridged plains was ~200 m and the total ice-shell thickness is >3000 m. This prediction is consistent with our proposed ice-shell thickening hypothesis, as the current ice shell is likely 20–30 km thick (e.g. Pappalardo et al., 1999; Schenk, 2002) implying a likely brittle layer thickness > 1 km (e.g., Carr et al., 1998; Nimmo and Manga, 2002; Spohn and Schubert, 2003; Nimmo and Schenk, 2006). Eventually, as the ice shell continued to thicken,

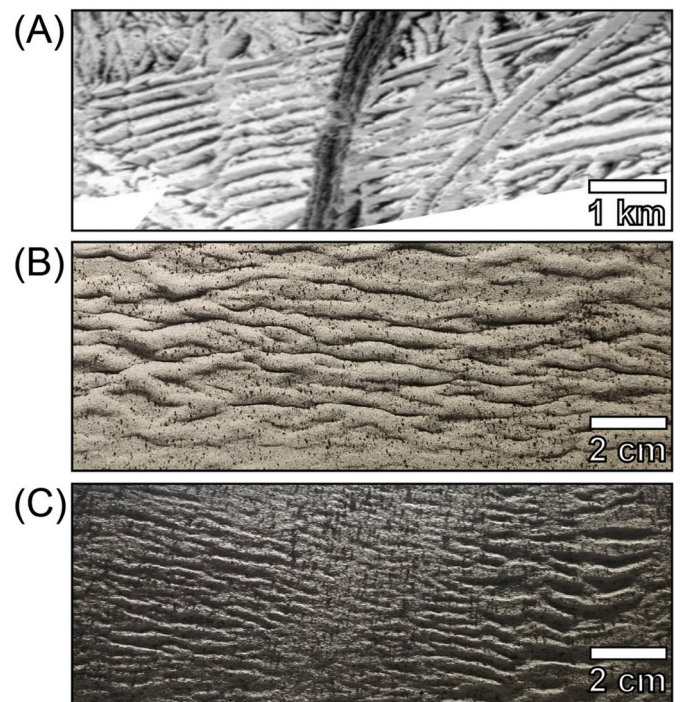


Fig. 11. Experiment results compared to ridged plains terrain in map view. The top panel (A) includes two frames (2400 and 2404) from the E12 MOTTLE mosaic of the subparallel ridge-and-trough morphology of the ridged plains. The middle panel (B) shows the results of a compression experiment with 0.5 cm brittle layer and 8 cm ductile layer. The bottom panel (C) shows the results of an extensional experiment with 0.5 cm brittle layer and 2 cm ductile layer.

Table 3
Europa ridged plains observations compared to analog model results.

Analogue Model	Compression Experiments	Extension Experiments
Rounded in cross-section	Y	P
Linear to curvilinear along length	Y	Y
Large length to width ratios (>10)	Y	Y
Narrow troughs	Y	N
Shallow (< 25) slopes	Y	N
Quasi-symmetrical slopes	Y	Y

Note: Green color ("Y") indicates where experiments satisfies the observation, red color ("N") indicates where it is not satisfied, and orange color ("P") indicates where it is unclear or partially satisfied.

extensional stresses dominated and ridged plains formation stopped. If this were the case, we would expect to observe signatures of an ice-shell that has thickened through time with the data returned by the Europa Clipper mission.

Acknowledgments

This work was supported by the NASA Earth and Space Science Fellowship Program – grant 80NSSC17K0602. Portions of this research were carried out at the Jet Propulsion Laboratory, California Institute of Technology, under contract with the National Aeronautics and Space Administration. This work was supported in part by NASA under the Europa Clipper Project.

References

- Beeman, M., Durham, W.B., Kirby, S.H., 1988. Friction of ice. *J. Geophys. Res.* 93, 7625–7633.
- Bierhaus, E.B., Chapman, C.R., 2009. Europa's crater distributions and surface ages. In: *Europa. The University of Arizona*, pp. 161–180.
- Broxton, M.J., Edwards, L.J., 2008. The Ames stereo pipeline: automated 3D surface reconstruction from orbital imagery, lunar planet. *Sci.* 39, 2419.
- Burov, E., Diament, M., 1995. The effective elastic thickness (T_e) of continental lithosphere: what does it really mean?, 100, 3905–3927.
- Carr, M.H., Bolton, M.J.S., Chapman, C.R., Davies, M.E., Geissler, P., Greenberg, R., McEwen, A.S., Tufts, B.R., Greeley, R., Sullivan, R., Head, J.W., Pappalardo, R.T., Klaasen, K.P., Johnson, T.V., Kaufman, J., Senske, D., Moore, J., Neukum, G., Schubert, G., Burns, J.A., Thomas, P., Veverka, J., 1998. Evidence for a subsurface ocean on Europa. *Nature* 391, 363–365. <https://doi.org/10.1038/34857>.
- Collins, G., Nimmo, F., 2009. Chaotic terrain on Europa. In: *Europa. The University of Arizona*, pp. 259–281.
- Crawford, G.D., Stevenson, D.J., 1988. Gas-driven water volcanism and the resurfacing of Europa. *Icarus* 73, 66–79.
- Cruz, L., Teyssier, C., Perg, L., Take, A., Fayon, A., 2008. Deformation, exhumation, and topography of experimental doubly-vergent orogenic wedges subjected to asymmetric erosion. *J. Struct. Geol.* 30, 98115. <https://doi.org/10.1016/j.jsg.2007.10.003>.
- Davy, P., Cobbold, P.R., 1988. Indentation tectonics in nature and experiment. 1. Experiments scaled for gravity. *Bull. Geol. Inst. Univ. Uppsala* 14, 129–141.
- Doggett, T., Greeley, R., Figueredo, P.H., 2009. Geologic stratigraphy and evolution of Europa's surface. In: *Europa*, pp. 137–159.
- Dubey, A.K., Cobbold, P.R., 1977. Noncylindrical flexural slip folds in nature and experiment. *Tectonophysics* 38 (3–4), 223–239.
- Figueredo, P.H., Greeley, R., 2004. Resurfacing history of Europa from pole-to-pole geological mapping. *Icarus* 167, 287–312. <https://doi.org/10.1016/j.icarus.2003.09.016>.
- Fletcher, R.C., Hallet, B., 1983. Unstable extension of the lithosphere: a mechanical model for basin-and-range structure. *Journal of Geophysical Research: Solid Earth* 1978–2012, 7457–7466. <https://doi.org/10.1029/JB088iB09p07457>.
- Greeley, R., Figueredo, P.H., Williams, D.A., Chuang, F.C., Klemaszewski, J.E., Kadel, S. D., Prockter, L.M., Pappalardo, R.T., Head, J.W., Collins, G.C., Spaun, N.A., Sullivan, R.J., Moore, J.M., Senske, D.A., Tufts, B.R., Johnson, T.V., Bolton, M.J.S., Tanaka, K.L., 2000. Geologic mapping of Europa. *Journal of Geophysical Research: Planets* (1991–2012) 105 (E9), 22559–22578. <https://doi.org/10.1029/1999JE001173>.
- Greenberg, R., Geissler, P., 2002. Europa's dynamic icy crust. *Meteorit. Planet. Sci.* 37 (12), 1685–1710. <https://doi.org/10.1111/j.1945-5100.2002.tb01158.x>.
- Greenberg, R., Geissler, P., Hoppa, G., Tufts, B.R., Durda, D.D., Pappalardo, R.T., Head, J. W., Greeley, R., Sullivan, R., Carr, M.H., 1998. Tectonic processes on Europa: tidal stresses, mechanical response, and visible features. *Icarus* 135, 64–78.
- Greenberg, R., Hoppa, G.V., Tufts, B.R., Geissler, P., Riley, J., 1999. Chaos on Europa. *Icarus* 141, 263–286.
- Head, J.W., Sherman, N.D., Pappalardo, R.T., Greeley, R., Sullivan, R., Senske, D., McEwen, A., the Galileo Imaging Team, 1998. Geologic history of the E4 region of Europa: implications for ridge formation, cryovolcanism, and chaos formation. In: *Lunar and Planetary Science XXIX*, pp. 6–7.
- Hoppa, G., Tufts, B.R., Greenberg, R., Geissler, P., 1999a. Strike-slip faults on Europa: global shear patterns driven by tidal stress. *Icarus* 141, 287–298. <https://doi.org/10.1006/icar.1999.6185>.
- Hubbert, M.K., 1937. Theory of scale models as applied to the study of geologic structures. *Geol. Soc. Am. Bull.* 48 (10), 1459–1520. <https://doi.org/10.1130/GSAB-48-1459>.
- Kattenhorn, S.A., 2002. Nonsynchronous rotation evidence and fracture history in the Bright Plains region, Europa. *Icarus* 157 (2), 490–506. <https://doi.org/10.1006/icar.2002.6825>.
- Kattenhorn, S.A., Prockter, L.M., 2014. Evidence for subduction in the ice shell of Europa. *Nat. Geosci.* 7, 762–767. <https://doi.org/10.1038/ngeo2245>.
- Leonard, E.J., Howell, S., 2019. Compositional variations within Europa's ice shell: implications for surface geology. In: *Lunar and Planetary Science Conference*, 50.
- Leonard, E.J., Pappalardo, R.T., Yin, A., 2018. Analysis of very-high-resolution Galileo images and implications for resurfacing mechanisms on Europa. *Icarus* 312. <https://doi.org/10.1016/j.icarus.2018.04.016>.
- Maillot, B., Koyi, H., 2006. Thrust dip and thrust refraction in fault-bend folds: analogue models and theoretical predictions. *J. Struct. Geol.* 28, 3649. <https://doi.org/10.1016/j.jsg.2005.10.001>.
- Manga, M., Sinton, A., 2004. Formation of bands and ridges on Europa by cyclic deformation: insights from analogue wax experiments. *Journal of Geophysical Research: Planets* 1991–2012, 109. <https://doi.org/10.1029/2004JE002249>.
- Martinod, J., Davy, P., 1994. Periodic instabilities during compression of the lithosphere 2. Analogue experiments. *Journal of Geophysical Research* 99 (10), 12057–12069. <https://doi.org/10.1029/93JB03599>.
- Michaut, C., Manga, M., 2014. Domes, pits, and small chaos on Europa produced by water wells. *Journal of Geophysical Research: Planets* 119 (3), 550–573. <https://doi.org/10.1002/2013JE004558>.
- Mitri, G., Showman, A.P., 2005. Convective-conductive transitions and sensitivity of a convecting ice shell to perturbations in heat flux and tidal-heating rate: implications for Europa. *Icarus* 177 (2), 447–460. <https://doi.org/10.1016/j.icarus.2005.03.019>.
- Moratto, Z.M., Broxton, M.J., Beyer, R.A., Lundy, M., Husmann, K., 2010. Ames stereo pipeline, NASA's open source automated stereogrammetry software, lunar planet. *Sci.* 41, 2364.
- Nimmo, F., 2004. Stresses generated in cooling viscoelastic ice shells: application to Europa. *Journal of Geophysical Research: Planets* 1991–2012, 109. <https://doi.org/10.1029/2004JE002347>.
- Nimmo, F., Manga, M., 2002. Causes, characteristics and consequences of convective diapirism on Europa. *Geophys. Res. Lett.* 29, 24. <https://doi.org/10.1029/2002GL015754>.
- Nimmo, F., Schenk, P., 2006. Normal faulting on Europa: implications for ice shell properties. *J. Struct. Geol.* 28, 21942203. <https://doi.org/10.1016/j.jsg.2005.08.009>.
- O'Brien, D., Geissler, P.E., Greenberg, R., 2002. A melt-through model for chaos formation on Europa. *Icarus* 156, 152–161. <https://doi.org/10.1006/icar.2001.6777>.
- Pappalardo, R.T., Greeley, R., 1995. A review of the origins of subparallel ridges and troughs: generalized morphological predictions from terrestrial models. *Journal of Geophysical Research: Planets* (1991–2012) 100 (E9), 18985–19007. <https://doi.org/10.1029/94JE02638>.
- Pappalardo, R.T., Head, J.W., Greeley, R., Sullivan, R.J., Pilcher, C., Schubert, G., Moore, W.B., Carr, M.H., Moore, J.M., Belton, M.J.S., Goldsby, D.L., 1998. Geological evidence for solid-state convection in Europa's ice shell. *Letters to Nature* 391 (6665), 365–368. <https://doi.org/10.1038/34862>.
- Pappalardo, R.T., Belton, M.J.S., Breneman, H.H., Carr, M.H., Chapman, C.R., Collins, G. C., Denk, T., Fagents, S., Geissler, P.E., Giese, B., Greeley, R., Greenberg, R., Head, J. W., Helfenstein, P., Hoppa, G., Kadel, S.D., Klaasen, K.P., Klemaszewski, J.E., Magee, K., McEwen, A.S., Moore, J.M., Moore, W.B., Neukum, G., Phillips, C.B., Prockter, L.M., Schubert, G., Senske, D.A., Sullivan, R.J., Tufts, B.R., Turtle, E.P., Wagner, R., Williams, K.K., 1999. Does Europa have a subsurface ocean? Evaluation of the geological evidence. *Journal of Geophysical Research: Planets* (1991–2012) 104 (E10), 24015–24055. <https://doi.org/10.1029/1998JE000628>.
- Patel, J.G., Pappalardo, R.T., Head, J.W., Collins, G.C., Hiesinger, H., Sun, J., 1999. Topographic wavelengths of Ganymede groove lanes from Fourier analysis of Galileo images. *J. Geophys. Res.* 104 (E10), 24057–24074.
- Patel, J.G., Pappalardo, R.T., Prockter, L.M., Collins, G.C., Head, J.W., Galileo SSI Team, 1999b. Morphology of ridge and trough terrain on Europa: Fourier analysis and comparison to Ganymede. *Eos Trans AGU* 80 (17), 210.
- Phillips, C.B., Pappalardo, R.T., 2014. Europa Clipper mission concept: exploring Jupiter's ocean moon. *Eos, Transactions American Geophysical Union* 95 (20), 165–167.

- Poirier, J.P., 1982. Rheology of ices: a key to the tectonics of the ice moons of Jupiter and Saturn. *Nature* 299, 683–687. <https://doi.org/10.1038/299683a0>.
- Prockter, L., Patterson, G., 2009. Morphology and evolution of Europa's ridges and bands. In: *Europa*. University of Arizona, pp. 237–258.
- Prockter, L.M., Pappalardo, R.T., 2000. Folds on Europa: implications for crustal cycling and accommodation of extension. *Science* 289 (5481), 941–943. <https://doi.org/10.1126/science.289.5481.941>.
- Prockter, L.M., Head, J.W., Pappalardo, R.T., Senske, D.A., Neukum, G., Wagner, R., Wolf, U., Oberst, J., Giese, B., Moore, J.M., Chapman, C.R., Helfenstein, P., Greeley, R., Breneman, H.H., Belton, M.J.S., 1998. Dark terrain on Ganymede: geological mapping and interpretation of Galileo Regio at high resolution. *Icarus* 135, 317344. <https://doi.org/10.1006/icar.1998.5981>.
- Prockter, L.M., Figueredo, P.H., Pappalardo, R.T., Head, J.W., Collins, G.C., 2000. Geology and mapping of dark terrain on Ganymede and implications for grooved terrain formation. *Journal of Geophysical Research: Planets* (1991–2012) 105, 22519–22540. <https://doi.org/10.1029/1999JE001179>.
- Prockter, L.M., Head, J.W., Pappalardo, R.T., Sullivan, R.J., Clifton, A.E., Giese, B., Wagner, R., Neukum, G., 2002. Morphology of European bands at high resolution: a mid-ocean ridge-type rift mechanism. *Journal of Geophysical Research: Planets* (1991–2012) 107 (E5), 4. <https://doi.org/10.1029/2000JE001458>.
- Riller, U., Cruden, A.R., Boutelier, D., Schrank, C.E., 2012. The causes of sinuous crustal-scale deformation patterns in hot orogens: evidence from scaled analogue experiments and the southern Central Andes. *Journal of Structural Geology*. Elsevier Ltd 37, 65–74. <https://doi.org/10.1016/j.jsg.2012.02.002>.
- Sarid, A.R., Greenberg, R., Hoppa, G.V., Hurford, T.A., Tufts, B.R., Geissler, P., 2002. Polar wander and surface convergence of Europa's ice shell: Evidence from a survey of strike-slip displacement. *Icarus* 158 (1), 24–41.
- Schenk, P.M., 2002. Thickness constraints on the icy shells of the Galilean satellites from a comparison of crater shapes. *Letters Nature* 417, 419–421. <https://doi.org/10.1038/417419a>.
- Schenk, P.M., McKinnon, W.B., 1989. Fault offsets and lateral crustal movement on Europa: evidence for a mobile ice shell. *Icarus*. Academic Press 79 (1), 75–100. [https://doi.org/10.1016/0019-1035\(89\)90109-7](https://doi.org/10.1016/0019-1035(89)90109-7).
- Schenk, P.M., Chapman, C., Moore, J., Zahnle, K., 2003. Ages and interiors: the cratering record of the Galilean satellites. In: Bagenal, F., McKinnon, W. (Eds.), *Jupiter: Planet, Magnetosphere, Satellites, and Magnetosphere*. Cambridge Univ. Press, Cambridge, UK.
- Schmidt, B.E., Blankenship, D.D., Patterson, G.W., Schenk, P.M., 2011. Active formation of “chaos terrain” over shallow subsurface water on Europa. *Nature* 479 (7374), 502–505. <https://doi.org/10.1038/nature10608>.
- Senske, D.A., Leonard, E.J., Patthoff, D.A., 2019. Geologic Mapping of Europa at Global and Regional Scales: Providing Comprehensive Insight into Crustal History and Evolution. In: *Lunar and Planetary Science Conference*, Vol. 50.
- Showman, A.P., Han, L., 2004. Numerical simulations of convection in Europa's ice shell: implications for surface features. *Journal of Geophysical Research* 109 (E1), E01010. <https://doi.org/10.1029/2003JE002103>. John Wiley & Sons, Ltd.
- Sims, D., Wyrick, D.Y., Ferrill, D.A., Morris, A.P., Collins, G.C., Pappalardo, R.T., Colton, S.L., 2014. Physical Models of Grooved Terrain Tectonics on Ganymede, pp. 3774–3778. <https://doi.org/10.1002/2014GL060359>.
- Smith, R.B., 1975. Unified theory of the onset of folding, boudinage, and mullion structure. *Geol. Soc. Am. Bull.* 86 (11), 1601. [https://doi.org/10.1130/0016-7606\(1975\)86<1601:UTOTOO>2.0.CO;2](https://doi.org/10.1130/0016-7606(1975)86<1601:UTOTOO>2.0.CO;2). GeoScienceWorld.
- Spencer, J.R., 1987. Thermal segregation of water ice on the Galilean satellites. *Icarus* 69, 297–313.
- Spohn, T., Schubert, G., 2003. Oceans in the icy Galilean satellites of Jupiter? *Icarus* 161 (2), 456–467.
- Stewart, S.A., 1996. Influence of detachment layer thickness on style of thin-skinned shortening. *J. Struct. Geol.* 18 (10), 1271–1274.
- Sullivan, R., Greeley, R., Homan, K., Klemaszewski, J., Belton, M.J.S., Carr, M.H., Chapman, C.R., Tufts, R., Head, J.W., Pappalardo, R.T., Moore, J., Thomas, P., the Galileo Imaging Team, 1998. Episodic plate separation and fracture infill on the surface of Europa. *Letters to Nature* 391, 371–373. <https://doi.org/10.1038/34874>.
- Wainwright, J.T., Brun, J.P., 1999. Narrow rifts versus wide rifts: inferences for the mechanics of rifting from laboratory experiments. *Philosophical Transactions of the Royal Society A: Mathematical, Phys. Eng. Sci.* 357 (1753), 695–712. <https://doi.org/10.1098/rsta.1999.0349>.
- Yin, A., 2000. Mode of Cenozoic east-west extension in Tibet suggesting a common origin of rifts in Asia. *Physics* 105, 745–759. <https://doi.org/10.1029/2000JB900168>.
- Zahnle, K., Schenk, P., Levison, H., Dones, L., 2003. Cratering rates in the outer solar system. *Icarus* 263–289. [https://doi.org/10.1016/S0019-1035\(03\)00048-4](https://doi.org/10.1016/S0019-1035(03)00048-4).
- Zuza, A.V., Yin, A., Lin, J., Sun, M., 2017. Spacing and strength of active continental strike-slip faults. *Earth and Planetary Science Letters* 457, 49–62. <https://doi.org/10.1016/j.epsl.2016.09.041>. Elsevier.